Numerical Investigation of Flame Propagation for Explosion Risk Modeling Development

Ashley M. Coates[a], Scott L. Lawrence[a], Donovan L. Mathias[a], and Brian J. Cantwell[b]
[a] NASA Ames Research Center, Moffett Field, USA, *ashley.m.coates@nasa.gov*
[b] Stanford University Aeronautics and Astronautics Dept., Stanford, USA, *cantwell@stanford.edu*

Abstract: Large, uncontained explosive failures in rocket engine bays pose significant danger to people and equipment in the surrounding area, establishing a need for risk assessments to be conducted. These assessments rely on several parameters, including the flame speed during propagation. The numerical study presented here further characterizes the flame speed by simulating flame propagation through a hydrogen-oxygen mixture and comparing simulation results with experimental data and engineering-level blast model results. The simulations consider variations in the initial pressure and velocity distribution to identify underlying parameters influencing the flame speed and investigate how these parameters may change the way results are used to inform risk assessment models. Numerical results show that flame speed increased as pressure increased, likely a result of increasing density, flame instability effects, and growing pressure waves in the confined domain. Adding a velocity distribution prior to ignition significantly increased the flame speed throughout the propagation and resulted in local accelerations as the flame interacted with underlying flow features. Comparisons with experimental data and engineering model results made clear that the presence and character of a non-uniform velocity field at ignition significantly affected the subsequent flame behavior and should be characterized. We conclude that the initial conditions of a scenario have a non-negligible effect on the flame speed and should be carefully reported for all numerical and experimental studies so that the results can be appropriately applied in the development of risk assessment models.

1. INTRODUCTION

One of the risks associated with large space launch vehicle systems is uncontained, explosive failures in the rocket engine bay. These failure scenarios pose a safety threat to crew, surrounding personnel, and equipment, making it necessary to conduct risk assessments that account for the possibility of these failures. Risk assessments completed using an engineering-level blast model are the fastest and most practical option for a physics-based probabilistic risk analysis, but more expensive (time, money, resources, safety) options like physical experiments or computational fluid dynamics (CFD) analyses are needed to inform the model development [1].

The current engineering-level blast risk model used in support of NASA's Space Launch System (SLS) program is analogous to the vapor cloud explosion model by Baker, Strehlow, and Tang (BST) [2]. Pressure wave propagation is an output of the model but selecting an appropriate flame speed for the scenario is a user input. Requiring the flame speed as an input is a limitation of the model and a driving factor for why flame speed and propagation characteristics are being further studied. The focus of the present work is to compare numerical results obtained from CFD simulations to experimental data for spherically expanding flame fronts and engineering-level blast model results for several scenarios. This work considers various pre-ignition features present in real scenarios or experimental setups, including filling and mixing processes, and highlights which parameters should be taken into consideration when using flame speed data for risk analysis models. The work presented here is part of a larger study [3] to examine parameters in the underlying flow that influence flame propagation and flame speed.

Numerical simulations and engineering model results computed by the authors and experimental data from tests conducted by the Hydrogen Unconfined Combustion Test Apparatus (HUCTA) team at Marshall Space Flight Center [4] will be used for these comparisons. Additional experimental [5–7]

and numerical [8–10] studies investigating large-scale deflagrations for accident scenarios involving hydrogen use and storage are available in the literature. Experimental setups described in the literature typically consist of a balloon or tent filled with a flammable mixture of gases that is ignited and allowed to propagate [4–7]. As the flame propagates towards the balloon walls, the container either pops or is cut allowing the flame and pressure waves to propagate freely through the gas and surroundings. Prior to ignition, a fan or recirculating pump is often used to mix the fuel and oxidizer to create an initially homogeneous mixture [4,6]. The process of filling and mixing the gas inside the container will be highlighted as an important parameter in the work presented here.

Numerical studies in the literature [8–10] modeling hydrogen deflagrations have had a variety of different approaches and setups. Setups include one and three dimensions, structured and unstructured meshes, different sub-models, and Euler, Reynolds-Averaged Navier-Stokes (RANS), and Large Eddy Simulation (LES) approaches. A summary of different approaches for modeling a given experimental data set is provided in [9]. At least partially driven by the computational cost of mesh refinement, the grid spacing can be relatively coarse, up to 4 m in some cases [8], which limits the simulations to capturing the gross features of the overall propagation. The work presented in this study aims to capture the smaller-scale details and determine how various parameters influence the flame front.

A review of actual vapor cloud explosions [11] found that most real accidents fall into either a large release rate, wind, and rapid ignition category, or a small release rate, no wind category. One of the conclusions from this review was that multiple parameters needed to be considered [11]. The presented work aims to determine how influential certain features are to determining the flame speed through a series of computational fluid dynamics simulations and comparisons with experimental data. Further comparisons with engineering model results highlight the importance of understanding the specifics of the setup of the experiments or computational simulations so that results can be appropriately applied in the development of an engineering model. The goal is to be able to inform an engineering-level risk assessment model, and a thorough understanding of the processes used to gain physical insight, including the initial setup, is required. The discovery of specific influential parameters will lead to better risk assessments in the future.

2. APPROACH

2.1. Code, Models, and Solver Parameters

The physics modeling of combustion problems can be quite complex. Flow instabilities, turbulence, and chemical reactions all need to be captured on large and small scales to produce reliable results. Resolving these flow aspects can lead to a computationally expensive, and in some cases impractical, set of simulations. Compromises are often made in areas such as chemistry modeling or mesh refinement to make studies more feasible. For this study, simulations were computed on a supercomputer using Loci-Chem [12,13], a highly parallelized computational tool that includes detailed chemical kinetics to limit simplifications in the modeling process. Loci-Chem is a density-based, finite-volume, unstructured solver with second-order accuracy in time and space. Capabilities include solving the Navier-Stokes equations for three-dimensional, viscous, turbulent, and chemically reacting flows, all of which are necessary for capturing the flame propagation scenarios studied here.

Several models and parameters were defined within the simulation setup to describe different aspects of the physics. A 7-species (H, O, H_2O, OH, O_2, H_2, and N_2), 8-reaction chemistry model by Evans and Schexnayder [14] with reaction rates defined by an Arrhenius equation was chosen for this study. This model was selected as a good compromise between simplified one-step reaction models, shown in the literature [15] to have limitations for flame propagation modeling, and more complex (and expensive) chemistry models. The built-in transportDB model [16] was selected for both the transport and diffusion models, and a Reynolds-Averaged Navier-Stokes approach with Menter's Baseline Model [17] was used for turbulence modeling. All simulations were unsteady and used time-accurate integration with both Gauss-Seidel and Newton iterations performed each time step. The finite volume approach used the Monotonic Upwind Scheme for Conservation Laws (MUSCL) scheme and the Barth flux limiter

[18] was applied to the extrapolation scheme because it was the most stable option at the higher pressures found in the combustion scenarios considered here. A complete discussion is provided in [3]. Further details on individual models in Loci-Chem are found in [16]. The combination of models and parameters described has been used in previous flame propagation work by the authors [19] and performed well.

2.2. Geometry and Mesh

The basic geometry for this set of simulations (Figure 1a) consisted of a 1.524 m diameter balloon mounted to structural pieces used to fill and ignite the gas mixture in the balloon, and was based on a set of experiments conducted at Marshall Space Flight Center known as the HUCTA experiments [4]. The experimental setup (Figure 1b) indicated that the balloon was filled from the base plate at the bottom of the balloon and a recirculation system, also at the base plate, was used to ensure a homogeneous mixture. A pole with the ignition system attached extended into the center of the balloon. In the simulation geometry, a 15.24 cm diameter base plate and a 2.54 cm diameter center pole were included to account for the internal structure of the experiment. Details on how the simulation accounted for the filling and recirculating of the gas at the base plate will be discussed in later sections. The shape of the balloon in the simulations was assumed to be spherical and axisymmetric to allow the use of a two-dimensional, axisymmetric mesh, reducing the cost of the simulations.

Figure 1: (a) Computational Setup and (b) HUCTA Experimental Setup [4]

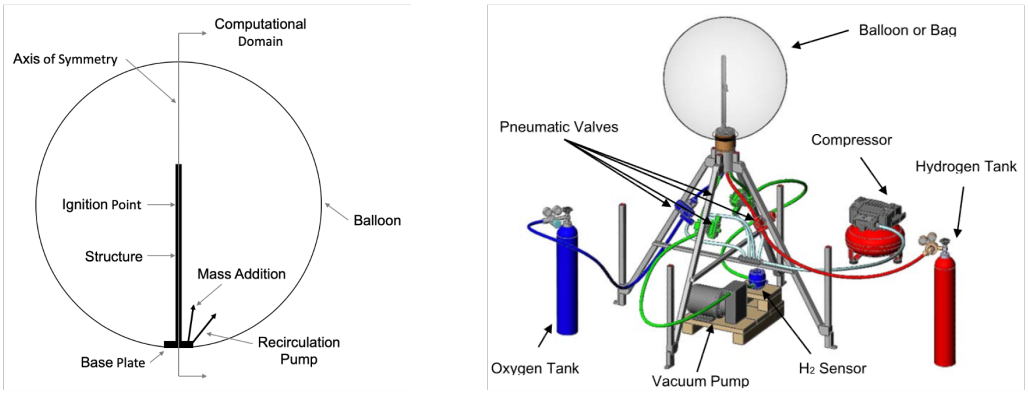

(a) (b)

Unstructured meshes were generated for the described two-dimensional domain [20]. The grid spacing required for capturing the flame front details was very small in comparison to the overall size of the domain, making the total number of elements in a uniform grid very large. To reduce the computational cost, meshes were generated with concentric rings of varying grid spacing (Figure 2). The section surrounding the flame front was the most refined and sections away from the flame front gradually increased in grid spacing. As the flame propagated to the edge of a refined mesh region, the solution was interpolated onto another mesh with the refined region shifted farther away from the ignition location to capture the next section of propagation. Regions behind the flame front were also coarsened as the flame propagated further from the ignition location. This manual mesh refinement method required generating multiple meshes and monitoring the flame front location to ensure it remained within a refined mesh region, but also allowed for more simulations to be conducted in a reasonable amount of time.

The laminar flame thickness for a hydrogen-oxygen mixture is reported by Ivanov et al. [21] to be between 0.26 mm and 0.32 mm, based on experimental and computed results, respectively. Therefore, the 0.254 mm grid spacing chosen for the most refined region around the flame front resulted in approximately 1 to 1.25 mesh cells within the laminar flame thickness. Coarser meshes were observed to produce significant flame speed inaccuracies compared to known laminar flame speeds, and finer meshes did not significantly improve the accuracy to warrant the extra computational costs.

Figure 2: Mesh Segment with Concentric Rings of Varying Grid Spacing

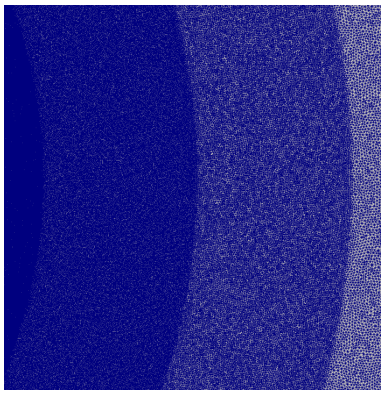

2.3. Boundary and Initial Conditions

The boundaries are labeled in Figure 1a. A requirement of the axisymmetric simulation is that the two-dimensional mesh be extruded one cell thick, creating front and back symmetry plane faces. The axis of symmetry was assigned an axisymmetric boundary condition and the pole structure was defined as an adiabatic no-slip wall. The balloon edge was defined as a stationary reflective boundary condition because the real problems of interest are rocket engine bay failures, which typically occur in a confined environment. In reality, the balloon would expand and pop as the flame propagated. Therefore, the choice of a reflective boundary condition makes the solution applicable to confined explosion scenarios and valid for comparison with experimental data up to the point of significant reflective pressure wave interactions. The boundary condition used at the base plate varied depending on the scenario. This boundary condition will be discussed just prior to the results of each study.

The initial pressure and velocity conditions also varied depending on the study and will be further discussed with each results section of the study. Generally, the balloon contained a premixed stoichiometric mixture of hydrogen and oxygen at approximately sea-level ambient conditions. The simulations included gravity with a downward acceleration of 9.8 m/s^2, though no stratification of the mixture was observed prior to ignition. Ignition, modeled by localized energy addition, occurred at the center of the balloon where the ignition source was mounted to the center pole as in the experiment. As energy was added, the gas in that area heated up and eventually started to burn, initiating the outward propagation of the flame through the balloon.

2.4. Verification and Validation

To ensure the described CFD code, models, and approach were sufficient for capturing the flame propagation problems of interest, a laminar flame at ambient conditions in a quiescent flow (baseline case for this study) was simulated using the current approach and compared to flame speeds generated with the Cantera chemistry tool suite [22] and the two-dimensional (to match the axisymmetric condition) power law for spherical flames [23]. This effort is described in [3], with the overall conclusion being that good comparisons were observed between the CFD results and both the Cantera model and the power law, establishing confidence that the code, models, and approach are sufficient for the study presented here. Future work should include investigating three-dimensional effects that may be neglected because of the quasi-two-dimensional nature of this study.

3. RESULTS AND DISCUSSION

The strength of pressure waves generated in a blast failure is dependent on the deflagration flame speed, making flame speed a necessary parameter in engineering-level risk assessment models. Whether using experimental data or computational results to inform the flame speed estimation, it is important to

understand the details and potential influences of the setup so that the results can be applied appropriately in the risk model. In the following sections, results of the numerical study will be presented along with comparisons with experimental data and engineering model results. Conclusions about influential parameters on flame speed will be discussed to further inform risk assessment models.

Throughout the study, the inertial flame speeds reported from the CFD simulations are determined by calculating the slope of a linear fit through the position versus time results of the flame propagation. Position at each time step was determined as the average of the distance from the ignition point to a point on the flame front for all points along the flame front. The flame front here was defined by a temperature contour at 1500 K.

3.1. Initial Pressure Variation

The first part of the study considered flame propagation in a quiescent environment with varying initial pressure. The goal was to characterize the effect of initial pressure on the flame propagation.

3.1.1. Additional Boundary and Initial Conditions

This part of the study assumed that the balloon was already filled with a hydrogen-oxygen mixture. The actual process of filling the balloon and recirculating the mixture was not modeled. As a result, the base plate was assigned an adiabatic no-slip boundary condition throughout the simulation. The mixture inside the balloon was initialized as a stoichiometric, premixed hydrogen-oxygen mixture in a zero-velocity quiescent environment. This assumed any movement initialized by the filling of the balloon (not modeled) had settled out prior to the start of the simulation. Initial temperature was set at a constant 300 K and initial pressure was varied from 101 kPa to 200 kPa. The initial temperature was held constant, so changes in initial pressure resulted in a corresponding change in initial density.

3.1.2. Flame Propagation

For each of the four initial pressures considered, the flame was ignited and allowed to propagate outward towards the balloon boundary. The time sequence images in Figure 3 display temperature contours for the 125 kPa case, where red represents hot burned gas and blue represents cooler unburned gas. Moving left to right through the three frames, the flame shape remained approximately spherical, with some wrinkling along the flame front forming due to instabilities. The instabilities likely started as a Darrieus-Landau instability, with Taylor instabilities likely involved in turbulence generated from the flame structure.

Figure 3: Temperature [K] Contour Sequence, Initially Quiescent with Pressure of 125 kPa

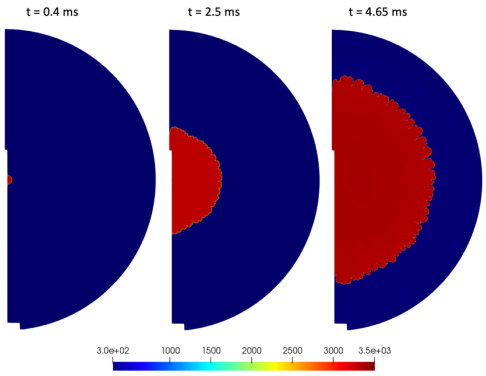

Flame propagation was consistent throughout the simulation for each case except when reflected pressure waves interacted with the flame in the later parts of the propagation. Pressure waves were induced ahead of the flame during propagation, eventually reaching the balloon surface and reflecting back towards the flame. Those waves eventually reached the center structure and reflected towards the

balloon surface, creating pressure waves traveling in both directions. These pressure waves can cause low magnitude deviations where the flame speed increases if the pressure wave traveled in the direction of the flame and decreases if the pressure wave moved in the opposite direction of the propagation. In reality it is unlikely that quite so many reflected pressure waves interacted with the flame because a balloon would have popped at some point.

The average flame speeds for the four cases with initial pressures of 101, 125, 150, and 200 kPa were computed as 89.0, 113.7, 141.7, and 226.2 m/s, respectively, a clear indication that flame speeds increased as initial pressure in the balloon increased. The faster flame speeds were likely a result of the increasing density of the mixture in the balloon, more mass means more fuel burning means more energy. Notably, the trend with the initial pressure was significantly stronger than was observed in the Cantera-generated laminar flame speeds for the same range of pressures. An increase of pressure from 101 kPa to 200 kPa produced approximately a 10-12% increase in the laminar inertial flame speed using the simple one-dimensional flow model. This seemed to indicate that a pressure or density effect on the growth rate of the flame instabilities could be occurring in the simulations. Preliminary FFT analyses suggested that while the frequency of instabilities was not significantly affected by pressure, there may have been a deepening of the instability valleys along the flame front as pressure increased. Increasing pressure in the balloon because of the balloon edge confinement was also a potential contributor.

3.2. Initial Velocity Variation

The second parameter considered was the initial velocity distribution (magnitude and flow pattern) in the balloon. Combustion failure scenarios can occur in environments with an underlying velocity distribution, and there is potential for experimental studies to introduce a velocity distribution through the filling and recirculation processes, making it an important parameter to consider for risk assessments. The goal here is to characterize potential effects that an initial velocity distribution has on the flame speed and determine how these effects could alter the way data is used in the development of engineering models.

3.2.1. Additional Boundary and Initial Conditions

The following simulations now attempted to model filling the balloon and recirculating the mixture by adjusting the boundary conditions at the base plate. To model these features, a velocity inlet condition was defined at the base plate where velocity and mass were added in two separate streams (ultimately rings because of the axisymmetric assumption). Multiple streams were chosen along the base plate to represent both the hydrogen-oxygen mixture being added as well as movement of the gas mixture introduced by the recirculation pump in the experiment. The balloon was considered filled when the total added mass equaled the mass in the quiescent case. Once the balloon was filled, the inlet condition was removed to prevent further velocity and mass addition. The base plate boundary condition was then defined as an adiabatic no-slip wall condition for the remainder of the simulation.

Figure 4: Streamlines Colored by Velocity Magnitude [m/s] for Three Initial Velocity Distributions

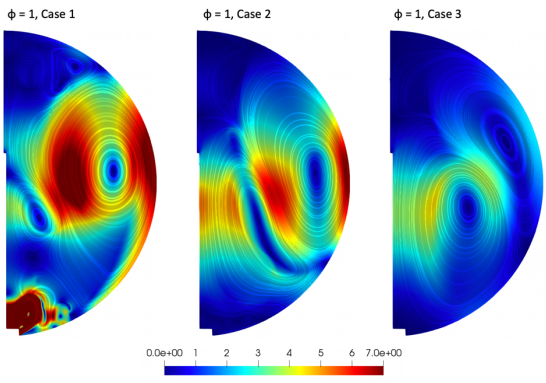

Modeling the filling process added some variability into the initial conditions. All simulations were initialized with a stoichiometric, premixed mixture of hydrogen and oxygen being added to ensure a homogeneous mixture prior to ignition. The velocity distributions that developed inside the balloon as velocity and mass were added were dominated by two large rotational features. Specific details regarding the filling process used in the experiment were not available. Because of this uncertainty, and because of our interest in the sensitivity to differences in the initial velocity field, three different initial velocity distributions were generated as pictured in Figure 4. After the simulated filling (same for all cases), the mixture was allowed to settle for different amounts of time to generate the three different distributions. Wait time between cases was equal to two-thirds the total fill time (t-fill). The longer the mixture was allowed to settle, the smaller the magnitude of the velocity distribution inside the balloon. The three different initial distributions are labeled Case 1 (no delay time), Case 2 (2/3 t-fill delay time), and Case 3 (4/3 t-fill delay time) with average velocity magnitudes of 3.25, 3.11, and 2.26 m/s, respectively. Any variations in pressure and temperature that were introduced into the domain during the filling process dissipated as the distribution was allowed to settle, resulting in very near uniform initial temperature and pressure fields. The initial average temperature and pressure were slightly raised in comparison to ambient conditions after the filling process. The experiments were conducted in open air, so it was assumed by the authors that the experiments were at approximately ambient conditions for initial pressure and temperature.

3.2.2. Flame Propagation

Compared to the results of the quiescent cases, the simulated flames in these cases propagated much faster and had regions of local acceleration and deformation resulting in a non-constant flame speed across the flame front. These characteristics of the flame propagation in the non-quiescent flows will be described in further detail throughout this section.

A time sequence of temperature contours showing an example of the flame propagation for the Case 2 velocity distribution is presented in Figure 5. The hot burned gas is represented by red and the cooler unburned gas by blue. Moving from left to right, the flame initially remained approximately spherical, but as the flame continued to propagate and interact with the underlying velocity field, the flame front deformed. A bulge along the flame front near the center of the domain is clear in frame three and resulted from the influence of the underlying flow field distribution. In regions where the flame developed local accelerations and deformed, the flame speed increased significantly. Flame instabilities formed along the flame front causing wrinkling as noted by the humps and cusps.

Figure 5: Temperature [K] Contour Sequence, Initially Case 2 Underlying Velocity Distribution

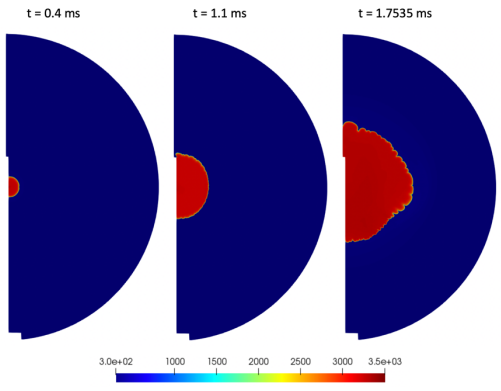

Streamlines for the Case 2 initial velocity field with the flame front propagation overlaid are pictured in Figure 6. The initial distribution streamlines, colored by the x-velocity (left) and the y-velocity (right) components, highlight two large features in the initial distribution, and the overlaid flame front propagation (white lines) provides insight into how the flame propagated and distorted when interacting with these underlying features. The initial features of the underlying velocity distribution may have compressed due to the flame-induced pressure waves ahead of the flame; however, the basic topology

of the distribution remained the same. Time between the contour lines of the overlaid flame propagation was constant, so equal spacing suggested a constant flame speed and increasing spacing suggested acceleration. Based on these flame front profiles, the flame initially had an approximately constant flame speed, but then accelerated and deformed as the flame interacted with the underlying flow, particularly near the center of the domain. Distortion of the flame front as the flame propagation progressed was especially evident in the +y and -x directions. The deformation in the +y direction corresponded with the region of high +y velocity in the underlying field near the center of the computational domain. A general shift in the -x direction occurred, matching the -x direction of the velocity distribution near the point of ignition and initial propagation. In general, it appeared that the underlying flow influenced the flame propagation and shape, with the flame accelerating in regions where the velocity distribution was in the same direction as the flame propagation and decelerating in regions of adverse flow.

Figure 6: Streamlines Colored by x-Velocity (Left) and y-Velocity (Right) [m/s] for the Case 2 Initial Velocity Distribution with Flame Front Locations Throughout Propagation Overlaid

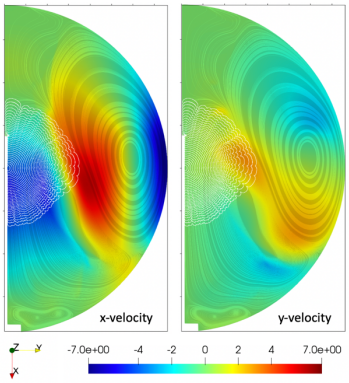

The average flame speeds over the propagation for Cases 1 (highest initial magnitude), 2, and 3, were computed as 196.9, 168.9, and 126.8 m/s, respectively. The simulation results clearly show an overall increased flame speed in comparison to the quiescent and Cantera results for the 101 kPa case. It is also clear that variations in the initial velocity distributions had a significant effect on the flame speed, causing differences of greater than 35% between Case 1 and Case 3. Further discussion on how the underlying flow distribution influenced the flame can be found in [3].

3.3. Comparison to Experiment

The initial pressure variation (Section 3.1) and initial velocity variation (Section 3.2) numerical results were compared with available experimental data. Note that the authors did not have complete information on the experimental test setup to inform specific initial and boundary conditions in the simulations so while comparisons are made, and plausible explanations discussed, concrete conclusions are not stated. Available experimental data included position data of the flame front along a line over time and the resulting average flame speed based on a linear fit of the position data. Mixture species, mixture ratio, container size, ignition location, and ignition spark duration were also provided for each case. Incomplete information on the pressure and temperature, filling and recirculation processes (fill time, mass flow rate, etc.), and settling time prior to ignition required the use of approximations for some initial and boundary conditions in the simulations. The range of results for both the numerical results and experimental data discussed highlight how influential the setup conditions are on the overall flame propagation.

Figure 7a plots the four flame speeds derived from the initial pressure variation simulations and a range of experimental data values. The range of experimentally observed flame speeds is represented by the gray band. The band extends across the range of simulated pressures because the exact initial pressure for the experiments was not reported. The flame speed range was determined by several experimental data points for approximately stoichiometric conditions. Experimentally derived flame speeds were all

significantly higher than the computed laminar flame speed at sea level conditions (84.29 m/s), suggesting that the flames in the experiment were either very turbulent or other parameters were influencing the flame speed. A linear fit of the simulation data points indicates that a 40% increase above ambient pressure would be needed to produce flame speeds similar to the experimental data using the quiescent flow environment setup. The balloons employed in these tests were obviously incapable of containing that level of pressure, suggesting pressure was not the driving parameter for the increased flame speed in the experimental data.

While the initial balloon pressure did not appear to explain the differences in flame speeds between the experimental test data and the laminar flame speed, other differences between the simulation model and the test procedure warranted examination. In particular, the potential for the test startup processes - filling the balloon and recirculating the mixture - to leave residual inhomogeneities in the velocity field appeared especially worthy of investigation, and bolstered plans to consider the effects of initial velocity variations on flame propagation.

Figure 7: Computational Flame Front Velocity Results for (a) Four Simulated Initial Pressures Compared to Near-Stoichiometric Experimental Data Range and (b) Three Simulated Initial Velocity Distributions Compared to Cantera-generated and Near-Stoichiometric Experimental Results

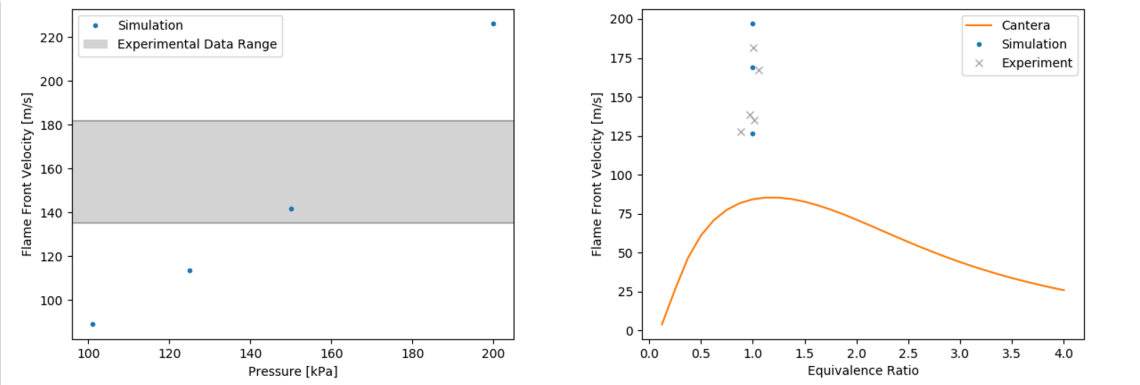

(a) (b)

Flame speed comparisons between the CFD results using the non-quiescent underlying velocity distributions, the experimental data for near stoichiometric conditions, and the laminar prediction by Cantera are presented in Figure 7b. The results clearly show that the non-quiescent environments increased flame speeds compared to the quiescent case, which closely matched the stoichiometric Cantera results, and that the specifics of the underlying velocity field had a significant effect on flame propagation. The range of simulated flame speeds now roughly corresponds to the values obtained from the test data. We emphasize that the simulations did not model the experiments exactly, since the experimental fill and recirculation process parameters were not reported and likely important. Consequently, no concrete conclusions are drawn regarding the underlying causes of the experimentally observed flame acceleration. However, it does seem clear that the presence and character of a non-uniform velocity field at ignition can significantly affect the subsequent behavior of the flame propagation and should be characterized.

Based on the results and comparisons presented thus far, it is apparent that the setup of an experiment, numerical or physical, can have a significant effect on the overall propagation of the flame. Simulations with several different initial conditions produced noticeably different flame speeds. The experimental data, which presumably had a similar process for every test case, also showed distinct variations in flame speeds. It is therefore crucial that results being provided for use in developing engineering-level models be clear about the process used to determine flame speed values so that they can be applied appropriately. This will be further highlighted in the next section where simulation results are compared to engineering-level blast model results.

3.4. Comparison to Engineering Level Blast Model

Available parameters for comparison between the simulation results and the engineering-level blast model results included flame front location over time and the pressure field over one-dimensional space. A pressure contour across one-dimensional space and time was created by extracting pressure information along a given line from each time step. A line perpendicular to the axis of symmetry extending from the ignition point out to the balloon edge was chosen to extract simulation results over time.

Comparison with the quiescent simulation results at an initial pressure of 101 kPa showed that the engineering model was well suited for capturing both the flame propagation and overpressure when the propagation remained effectively one-dimensional (generally spherical shape and approximately constant speed), and the flame speed was generally known. Based on these results, if the flame speed is known, pressure appears to be well resolved by the engineering model.

Figure 8: (a) Pressure Contours Tracking Changes Along a Given Line Over Time for the Case 2 Initial Velocity Distribution with Engineering Model Results Overlaid and (b) Computational Results for the Case 2 Initial Velocity Distribution Compared to Engineering Model Results for Pressure Along a Given Line at t=0.5 ms

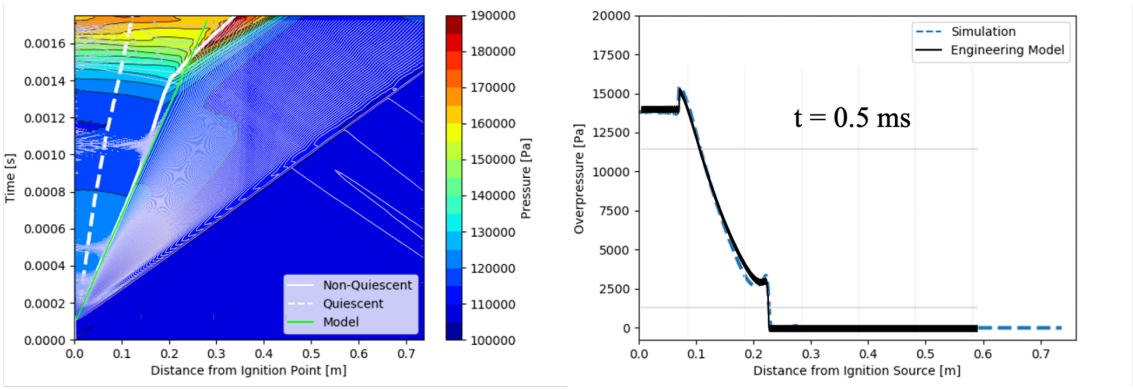

(a) (b)

The local accelerations and flame shape deformations occurring in the non-quiescent flows makes using the engineering model more challenging because it is harder to know what to choose as the flame speed. A comparison of the engineering model and the simulated flame propagation results corresponding to the Case 2 velocity distribution is shown in Figure 8a to illustrate the added challenges. Pressure contours are overlaid with the flame front location along the specified line over time (solid white line) for the Case 2 scenario. For comparison, the ambient quiescent propagation (dotted white line) is also included. The colored pressure contours to the right of the flame front line (solid white line) represent the induced pressure waves that traveled ahead of the flame front during propagation, and to the left represent the pressure field in the burned region. The non-quiescent case clearly accelerated and decelerated along the chosen line as indicated by the slope changes of the solid line and propagated faster than the quiescent case. Now consider the overlaid engineering level blast model results in Figure 8a. The engineering model was tuned in these comparisons to match the flame speed observed in the simulation during the initial part of the propagation. The flame propagation (green line) and induced pressure waves (gray contours) ahead of the flame did match well between the two sets of results for the initial part of the propagation before significant interactions with underlying flow features, but the model did not capture the changes in flame speed (slope) observed in the CFD results later in the propagation. Deviations later in the propagation highlight that additional input is required to capture the non-constant flame speed propagation resulting from the non-quiescent flow environment. To highlight the good comparison between the model and simulation in the initial part of the flow where the flame speed remained approximately constant, a line plot showing pressure (Figure 8b) is presented for both the model and simulation at a time of 0.5 ms where the flame front was approximately 7.62 cm from

the ignition point. The peaks matched well, again suggesting that if velocity is known then overpressure will be appropriately determined by the model.

The good agreement of the flame position and associated pressure waves between the model and simulation in the initial propagation provides validation of the model and confidence in the simulation approach. Because the overpressure continued to be well captured by the engineering model when the flame speed was correct, the focus for furthering the model capabilities should be placed on determining appropriate flame speeds, particularly in cases that are likely to deviate from effectively one-dimensional. Possible approaches for capturing flame speeds outside of the effectively one-dimensional case could include defining an average flame speed across the propagation, or using specific flow features as indicators of potential flame acceleration. These findings again highlight the need to truly understand the conditions under which results were obtained so that flame speed results guiding the engineering model can be applied appropriately.

4. CONCLUSION

The work presented in this paper aimed to identify problem setup features with the potential to influence flame propagation results. Numerical simulations were computed for a variety of initial conditions and compared to both experimental data and engineering model results. Understanding gained about important aspects of the experimental or computational setups improve how results are used and lead to more informed flame speed numbers, and ultimately improved risk assessments.

Two main parameters of the underlying flow were considered - pressure and velocity distribution. Varying the initial pressure (and density) in a quiescent flow revealed the clear trend that increased pressure led to faster flame speeds but was insufficient to capture the experimental flame speed data. Introducing an underlying velocity distribution also had a large effect on the results, with higher initial velocity magnitudes leading to faster flame speeds. It was evident that flame speed during the propagation was sensitive to flame interactions with the underlying flow features in the non-quiescent cases. The resulting regions of flame front acceleration led to challenges for the engineering model. However, if the flame speed was well-defined, the model was well-suited to capture blast wave overpressures.

Based on these results, there is a clear argument that both experimental and computational studies informing risk assessment models should be careful to report complete information on the setup and initial conditions used to produce results. Many experiments, like the one used here, use a recirculation system to mix the fuel and oxidizer until a homogeneous mixture forms, yet do not report information on settling times or the potential for a velocity distribution to be present prior to ignition. Computational studies can be guilty of this as well, neglecting to state approximations or assumptions when modeling given scenarios. Sufficient reporting of information on how flame speed results were obtained certainly matters for use in informing rocket engine bay risk analyses, but also for any relatively confined industrial setting where explosion hazards and the potential for flame propagation exists.

Acknowledgements

Supercomputing resources supporting this work were provided by the NASA High-End Computing (HEC) program through the NASA Advanced Supercomputing (NAS) Division at NASA Ames Research Center. The authors would also like to thank the HUCTA team at the NASA Marshall Space Flight Center for providing experimental data.

References

[1] S.L. Lawrence and D.L. Mathias. "*Blast overpressure modeling enhancements for application to risk-informed design of human space flight launch abort systems*", Reliability and Maintainability Symposium (RAMS), (2008).

[2] M.J. Tang and Q.A. Baker. "*A new set of blast curves from vapor cloud explosion*", Process Safety Progress, 18, pp. 235–240, (1999).
[3] A.M. Coates. "*Computational Flame Propagation Studies in Support of Launch Vehicle Risk Assessment*", PhD thesis, Stanford University, (2020).
[4] E. Richardson, T. Skinner, J. Blackwood, M. Hays, M. Bangham, and A. Jackson. "*An experimental study of unconfined hydrogen/oxygen and hydrogen/air explosions*", 46th Joint Army-Navy-NASA-Air Force (JANNAF) Combustion Conference, (2014).
[5] M. Groethe, E. Merilo, J. Colton, S. Chiba, Y. Sato, and H. Iwabuchi. "*Large-scale hydrogen deflagrations and detonations*", International Journal of Hydrogen Energy, 32, pp. 2125–2133, (2007).
[6] H. Schneider and H. Pfortner. "*Prozebgasfreisetzung-explosion in der gasfabrik and auswirkungen von druckwellen auf das containment*", Fraunhofer-ICT Internal Report: PNP-Sichcrheitssofortprogramm, (1983).
[7] K. Wakabayashi, T. Mogi, D. Kim, T. Abe, K. Ishikawa, E. Kuroda, T. Matsumura, Y. Nakayama, S. Horiguchi, M. Oya, and S. Fujiwara. "*A field explosion test of hydrogen-air mixtures*", International Conference on Hydrogen Safety, (2005).
[8] V. Molkov, D. Makarov, and H. Schneider. "*LES modelling of an unconfined large-scale hydrogen-air deflagration*", Journal of Physics D: Applied Physics, 39, pp. 4366–4376, (2006).
[9] J. Garcia, D. Baraldi, E. Gallego, A. Beccantini, A. Crespo, O.R. Hansen, S. Hoiset, A. Kotchourko, D. Makarov, E. Migoya, V. Molkov, M.M. Voort, and J. Yanez. "*An intercomparison exercise on the capabilities of CFD models to reproduce a large-scale hydrogen deflagration in open atmosphere*", International Journal of Hydrogen Energy, 35, pp. 4435–4444, (2010).
[10] V.V. Molkov, D.V. Makarov, and H. Schneider. "*Hydrogen-air deflagrations in open atmosphere: Large eddy simulation analysis of experimental data*", International Journal of Hydrogen Energy, 32, pp. 2198–2205, (2007).
[11] G. Atkinson, E. Cowpe, J. Halliday, and D. Painter. "*A review of very large vapour cloud explosions: Cloud formation and explosion severity*", Journal of Loss Prevention in the Process Industries, 48, 367– 375, (2017).
[12] E. Luke and T. George. "*Loci: A rule-based framework for parallel multidisciplinary simulation synthesis*", Journal of Functional Programming, 15, pp. 477–502, (2005).
[13] E. Luke. "*On robust and accurate arbitrary polytope CFD solvers (invited)*", 18th AIAA Computational Fluid Dynamics Conference, (2007).
[14] J.S. Evans and C.J. Schexnayder. "*Influence of chemical kinetics and unmixedness on burning in super-sonic hydrogen flames*", AIAA Journal, 18, pp. 188–193, (1980).
[15] M.F. Ivanov, A.D. Kiverin, I.S. Yakovenko, and M.A. Liberman. "*Hydrogen-oxygen flame acceleration and deflagration-to-detonation transition in three-dimensional rectangular channels with no-slip walls*", International Journal of Hydrogen Energy, 38, pp. 16427–16440, (2013).
[16] E.A. Luke, X. Tong, J. Wu, P. Cinnella, and R. Chamberlain. "*CHEM 3.3: A Finite-Rate Viscous Chemistry Solver - The User Guide*", (2014).
[17] F.R. Menter. "*Two-equation eddy-viscosity turbulence models for engineering applications*", AIAA Journal, 32, pp. 1598–1605, (1994).
[18] T.J. Barth and D.C. Jespersen. "*The design and application of upwind schemes on unstructured meshes*", 27th AIAA Aerospace Sciences Meeting, (1989).
[19] A.M. Coates, D.L. Mathias, and B.J. Cantwell. "*Numerical investigation of the effect of obstacle shape on deflagration to detonation transition in a hydrogen-air mixture*", Combustion and Flame, 209, pp. 278–290, (2019).
[20] Pointwise, Inc., https://www.pointwise.com/.
[21] M.F. Ivanov, A.D. Kiverin, and M.A. Liberman. "*Flame acceleration and DDT of hydrogen-oxygen gaseous mixtures in channels with no-slip walls*", International Journal of Hydrogen Energy, 36, pp. 7714– 7727, (2011).
[22] Cantera, https://cantera.org.
[23] M.A. Liberman, M.F. Ivanov, O.E. Peil, D.M. Valiev, and L-E Eriksson. "*Self-acceleration and fractal structure of outward freely propagating flames*", Physics of Fluids, 16, pp. 2476–2482, (2004).